ELSEVIER

Catalysis Today 33 (1997) 323–334

CATALYSIS TODAY

Effect of initial nickel and iron oxide morphology on their structural transformation in CO/H_2 mixture

O.S. Morozova [a,*], O.V. Krylov [a], G.N. Kryukova [b], L.M. Plyasova [b]

[a] *Semenov Institute of Chemical Physics [1], Russian Academy of Sciences, ul. Kosygina 4, Moscow 117334, Russian Federation*

[b] *Boreskov Institute of Catalysis [2], Siberian Branch of Russian Academy of Sciences, prosp. Lavrentjeva 5, Novosibirsk 630090, Russian Federation*

Abstract

The NiO and α-Fe_2O_3 samples from various backgrounds were used as precursors of the catalysts for CO hydrogenation. The effect of the initial microstructure of oxides on the morphological peculiarities and catalytic properties of the newly formed catalysts was studied using transmission electron microscopy and in situ XRD combined on-line with gas-chromatographic analysis. The initial morphology of precursors is found to be responsible for the direction and regularity of the solid–gas reactions yielding the catalyst, as well as for the 'architecture' and activity of the catalysts obtained: (i) NiO with the best developed plane (111) transforms into Ni_3C/NiO catalyst consisting of platelet oxide particle covered by Ni_3C microcrystals and producing the equal amounts of CH_4 and CO_2; disordering of the plane (111) induced by SD + HP leads to the formation of $Ni/Ni_3C/NiO$ catalyst consisting of the polycrystalline phases, whose catalytic properties improved; (ii) NiO with the best developed plane (100) transforms into $Ni/Ni_3C/NiO$ catalyst containing NiO microcrystals covered by Ni(100) and polycrystalline Ni_3C and giving CH_4 as a major product of reaction; action of SD + HP results in the formation of $Ni/Ni_3C/NiO$ catalyst containing polycrystalline Ni and Ni_3C phases, whose catalytic properties degraded. Similar correlation is observed for the catalysts prepared from α-Fe_2O_3.

Keywords: Nickel oxides; Iron oxides; Transmission electron microscopy; In situ X-ray diffraction; CO hydrogenation; Solid–gas reaction; Solid-phase transformation

1. Introduction

Topotactic reactions are found to be very important in solid state transformations including the preparation of catalysts [1–4]. As we recently reported, the initial microstructure of the oxide precursor determines both the solid-phase transformations resulting in the catalyst formation and the 'architecture' and catalytic properties of the sample obtained [5–7]. We explain these phenomena through the structural similarities being observed between initial and product solid phases. The following experimental results support our conclusions: (i) under the treatment by a CO/H_2 reaction mixture, the NiO sample with the best developed (111) plane gives the Ni_3C/NiO catalyst consisting of platelet oxide particles covered by Ni_3C 'monocrystals' and separate carbide particles; (ii) under similar conditions, the sample of NiO with

* Corresponding author.
[1] FAX: 7(095) 938-2156.
[2] FAX: 7(383)235-5756.

PII S0920-5861(96)00105-8

the best developed (100) plane gives the $Ni/Ni_3C/NiO$ catalyst consisting of faceted cubic NiO microcrystals covered by Ni (100) layers and polycrystalline Ni_3C; (iii) the catalysts possess different catalytic properties [6]; (iv) during the CO hydrogenation, two samples of α-Fe_2O_3 with different morphology give the χ-Fe_5C_2/Fe_3O_4 catalysts of varying 'architecture' and catalytic properties [7].

To prove our suggestion, we included into the investigations the samples of NiO and α-Fe_2O_3 subjected to shear deformation under high pressure (SD + HP). The shear deformation under high pressure on the Bridgeman anvil was used for disruption of the surface and bulk microstructure of oxides to verify the effect of initial microstructure on the peculiarities of solid-phase transformations.

The CO hydrogenation seems to be of special interest due to the participation of CO and H_2 in both the solid-phase and catalytic reactions.

With this aim, the long-term monitoring of both the structural and catalytic properties of the samples was carried out using an in situ high temperature X-ray diffraction technique (XRD) combined on-line with a gas chromatograph. On different stages of transformation, the morphology of the samples was studied using transmission electron microscopy (TEM).

In the present work, we review our results concerning the following aspects of the solid–gas reactions: (i) the effect of morphology of nickel and iron oxides on the direction and regularity of the solid-phase transformations; (ii) the effect of initial morphology of NiO and α-Fe_2O_3 precursors on the phase composition, microstructure, and the catalytic properties of the catalysts obtained.

2. Experimental

The preparation techniques and some properties of the polycrystalline powder samples being used are presented in Table 1 [8]. The experimental procedure was described in detail previ-

Table 1
Description of NiO and α-Fe_2O_3 samples

Sample	Preparation procedure	Morphological features	Surface area (BET) (m^2 g^{-1})	Average particle size (TEM), Å	Microstrain density
NiO(C-1)	Air calcination of $NiCO_3$ (Merk) at 700°C for 5 h	Platelets with (111) best developed planes, surface steps on lateral sides	4.9	1500	0.002
NiO(C-2)	NiO(C-1) subjected to SD + HP on Bridgeman anvil, 20 kbar, 140°C, cycle regime	Well-developed dislocation network, disordered surface structure of the close packed plane	1.6	800	0.007
NiO(P-1)	Plasmochemical method [8]	Cubic microcrystals with the (100) best developed planes, broad variation in particle size: 200–2000 Å	20.0	400	< 0.001
NiO(P-2)	NiO(P-1) subjected to SD + HP on Bridgeman anvil, 20 kbar, 140°C, cycle regime	Cubic microcrystals broken lengthwise of (111) plane, destruction of large microcrystals into the smaller ones	7.2	200	0.0025
α-Fe_2O_3(I)	Analytical grade	Platelets with the best developed (0001) basal plane, layered structure	9.0	1000	
α-Fe_2O_3(II)	α-Fe_2O_3(I) subjected to SD + HP on Bridgeman anvil, 20 kbar, 140°C, cycle regime	Disturbances in the layer packing, disordering of microblocks without crushing the particle as a whole	10.0	2000	

ously [5–7]. The structural–catalytic tests were carried out at atmospheric pressure with the unreduced samples, which were placed into the flow thermochamber for XRD measurements or into the heated flow reactor cell for simultaneous monitoring of the structural and catalytic properties. The initial sample was heated in a flow of He up to a chosen temperature. Thereafter, He was replaced by the reaction mixture of CO and H_2 ($CO:H_2 = 1:1.5$) with a total flow rate of 6 ml min^{-1}. The changes in the phase composition of the catalyst and in the composition of the reaction mixture on the outlet of the reactor were registered simultaneously every 10 or 20 min, as dictated by the rates of solid-phase and catalytic reactions. The reaction temperatures varied in the range of 195–285°C for the NiO samples and in the range of 270–360°C for the α-Fe_2O_3 samples.

Two kinds of experiments were carried out: under non-steady-state and steady-state conditions. In the first case, a 1-h treatment of the sample in the reaction mixture at the given temperature took place. Then, the temperature was raised by 15°C and the run was carried on at the higher temperature, as before. In the second case, the treatment was continued at the given temperature until the steady state of the solid-phase and catalytic processes was achieved. Thereafter, the temperature was raised by 15°C and the run was prolonged until a new steady state was observed.

To study the kinetics of the phase transformation, we systematically recorded the XRD patterns containing the characteristic peaks of NiO, Ni, and Ni_3C or α-Fe_2O_3, Fe_3O_4, and χ-Fe_5C_2. A scan speed of 1°/min was used. The phase compositions of the catalysts were verified by the JSPDC data files. The relative concentrations of different phases in the sample were calculated on the basis of integral intensities of the characteristic diffraction peaks. X-ray spectra were obtained with a D-500 Siemens diffractometer fitted with an HTK-10 Anton Paar thermochamber for in situ investigations and with a Dron-2 diffractometer furnished with a home-made flow reactor cell for simultaneous structural and catalytic measurements [9]. Monochromatized Cu K_α or Fe K_α radiation were used as X-ray sources. The microstructure of the initial samples and samples subjected to SD + HP was studied using XRD and TEM techniques. The time-counting XRD spectra were obtained using a HZG-4 diffractometer. The microstrain density was calculated by the method given in [10]. TEM investigation were carried out using a JEM-100 CX electron microscope with 0.3 nm resolution and accelerating potential of 100 kV. The samples were prepared from an ethanol suspension and deposited onto the copper grids covered by an amorphous carbon film.

3. Results and discussion

3.1. 'Carbonate' NiO samples

According to TEM data (Fig. 1, top left), the microcrystals of the initial NiO(C-1) sample have the form of thin platelets with the most developed (111) plane, as was shown by electron microdiffraction. The surface steps are present on the lateral sides of the oxide particles. Microcrystals of the NiO(C-2) sample subjected to SD + HP (Fig. 1, top right) are characterized by a well-developed dislocation network. The concentration of lattice defects is so high (see Table 1) that the 'monocrystalline' structure of the NiO particle is transformed into a 'polycrystalline' one.

Interaction of the initial sample with a CO/H_2 reaction mixture at 240–285°C results in the formation of Ni_3C (Fig. 2a). The phase of metallic Ni is not detected during the tests. The peculiarities of solid-phase transformation under the reaction conditions are described in [6]. As is exhibited by TEM, the microcrystals of Ni_3C appeared on the surface of the NiO(C-1) microcrystals in the form of regular hexagonal platelets. When the 'monocrystalline' platelet of Ni_3C occupies the whole (111) surface of the oxide particle, it leaves the 'parent' microcrys-

tal promoting the formation of a new Ni_3C particle. The crystallographic orientation similarity between the most developed (111) plane of NiO(C-1) and the (0001) basal plane of the hexagonal unit cell of Ni_3C leads to Ni_3C formation only when the definite amount of carbon atoms ($C_{intrinsic}$) accumulates in the subsurface layer of the oxide microcrystal [11]. The $C_{intrinsic}$ can be produced by the following reactions:

$$CO + O_{lat} \rightarrow CO_2 + V_{lat} \quad (1)$$

$$CO + V_{lat} \rightarrow C_{intrinsic} + O_{lat} \quad (2)$$

$$CO \rightarrow C_{intrinsic} + CO_2 \quad (3)$$

$$CO_{ads} + CO_{ads} \rightarrow C_{intrinsic} + CO_2, \quad (4)$$

were O_{lat} and V_{lat} are the lattice oxygen and oxygen vacancy, respectively; CO_{ads} is a molecule of CO adsorbed.

Thus, the Ni_3C/NiO sample consisting of the 'monocrystalline' components is the product of solid-phase transformation of the NiO(C-1) sample in a CO/H_2 mixture.

The catalytic activity of the NiO(C-1) sample is found to be observed at 285°C. Table 2 summarizes the results of catalytic and XRD experiments. Low values of CO conversion and CH_4 formation rate are observed before Ni_3C is produced. When the Ni_3C phase appears, the conversion of CO, as well as the rates of CH_4 and CO_2 formation, increase proportionally to the content of carbide in the sample.

Of special note is a very high rate of CO_2 formation being observed during all of the experiments performed for the initial 'carbonate' sample and for the Ni-containing sample specially prepared from the initial one [5]. We assume that the interface between NiO and Ni_3C is highly favourable for the CO_2 formation. On

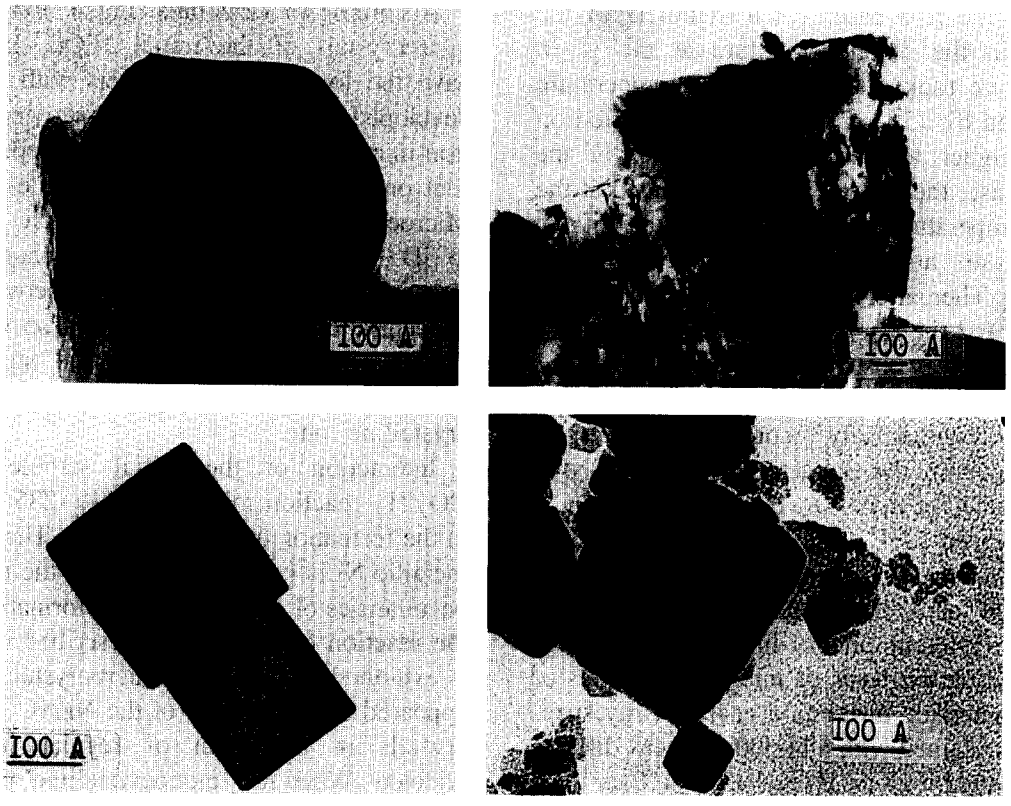

Fig. 1. TEM micrographs of (top left) initial 'carbonate' sample, (top right) 'carbonate' sample subjected to SD + HP, (bottom left) initial 'plasmochemical' sample, and (bottom right) 'plasmochemical' sample subjected to SD + HP.

the other hand, the low hydrogenation activity could be attributed to deficiency of centers for H_2 activation on the catalysts consisting of the oxide and carbide phases of special morphology.

After the action of SD + HP, a well-developed dislocation network is observed on the surface of the NiO(C-2) microcrystals. The disordered 'polycrystalline' surface structure of the (111) close packed plane has no structural similarity with the (0001) basal plane of Ni_3C. As a result, the NiO(C-2) sample is reduced to polycrystalline Ni at 240°C. In contrast to the initial NiO(C-1), the phase of Ni_3C is not observed (Fig. 2b). We assume that a great number of unsaturated Ni atoms appear in the vicinity of dislocation exits on the (111) plane, which are the centers of Ni nucleation. At 255°C, carbidization of the Ni phase into polycrystalline Ni_3C takes place.

Thus, the interaction of NiO(C-2) with a CO/H_2 mixture gives the multicomponent sample $Ni/Ni_3C/NiO$ containing the polycrystalline phases of Ni and Ni_3C. In response to the mechanically induced defects in the initial microstructure, both direction and regularity of the solid state reactions are changed.

The dynamics of catalytic and structural properties of $Ni/Ni_3C/NiO$ is shown in Table 2. Mechanical activation of the NiO(C-1) precursor improved the catalyst being prepared: the conversion of CO, as well as the CH_4 and CO_2 formation rates, increased several times, as compared to those on the Ni_3C/NiO sample. The fraction of hydrocarbons in the reaction products also increased. The presence of the metal phase is not the only reason of the catalyst improvement. A comparison between two $Ni/Ni_3C/NiO$ samples being prepared from NiO(C-1) and NiO(C-2) precursors shows that the second one with low Ni content has a better catalytic properties.

Consequently, not only the phase composition of a sample, but also the microstructure and morphology of the separate phase are important for the explanation of the catalyst behaviour.

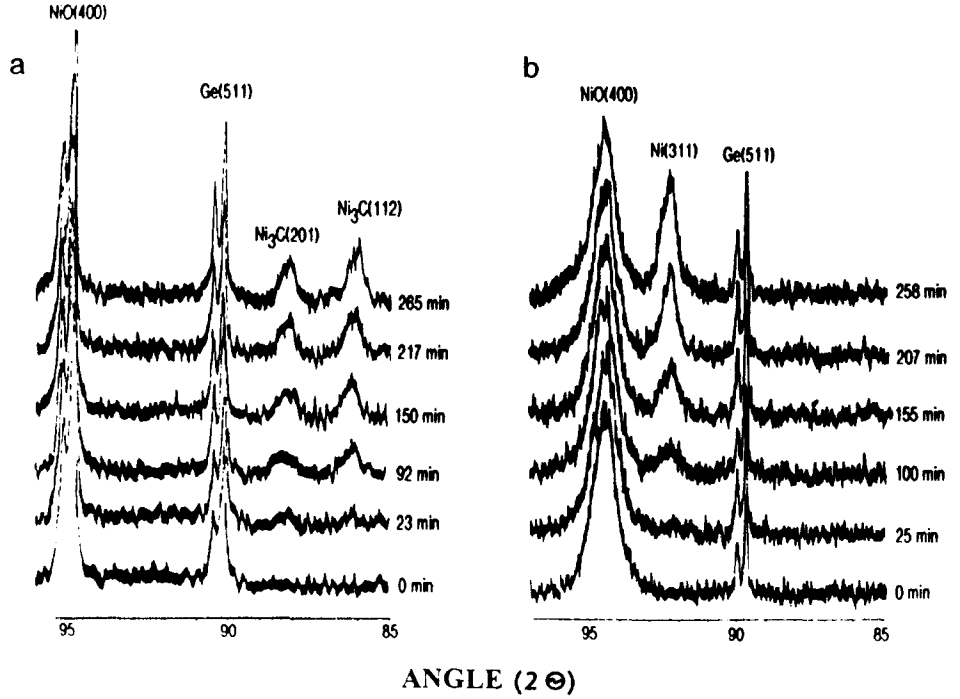

Fig. 2. In situ XRD spectra obtained during the reaction of a CO/H_2 mixture with (a) NiO(C-1) and (b) NiO(C-2) at 240°C.

Unfortunately, our experimental data are insufficient for this discussion.

3.2. *'Plasmochemical' NiO sample*

According to TEM micrographs (Fig. 1, bottom left), the initial NiO(P-1) sample consists of perfectly shaped cubic microcrystals of various size with a high concentration of point defects [6,12]. Microdiffraction data indicate that the (100) plane is the most developed one. Fig. 1, bottom right, shows the effect of SD + HP on the microstructire of the initial sample. Under the action of SD + HP, the major part of the large and medium-sized microcrystals breaks apart along the [100] direction transforming into smaller ones. A portion of these microcrystals is found to be broken along the (111) plane. The small microcrystals generally keep the perfect cubic shape.

Interaction of the NiO(P-1) sample with a CO/H_2 reaction mixture at 190–240°C results in a partial reduction into metal Ni (Fig. 3a). According to TEM data, the layers of metal nickel(100) are formed on the surface of the NiO particles because of the orientation relationship $[100]_{Ni}/[100]_{NiO}$. The peculiarities of the reduction process were described in detail in [6]. When the fast-reacting small microcrystals were reduced into Ni, the reconstruction of the (100) plane of the large microcrystals was still in progress. The surface steps and facets were found to be formed lengthwise on the (111) plane of NiO. According to Buckett and Marks [13], the destruction of the (100) plane took place under the action of carbon clusters. We

Table 2
Dynamics of structural and catalytic properties of the initial 'carbonate' NiO samples and the sample subjected to shear deformation under high pressure, 285°C

t [a] (min)	Conversion CO (%)	Selectivity [b] (%)			Rate (mol s^{-1} m^{-2})			Phase composition (mol%)		
		CH_4	C_2H_6	CO_2	10^8 CH_4	10^9 C_2H_6	10^8 CO_2	Ni	Ni_3C	NiO
Initial sample A. NiO										
30	0.55	23.8	–	66.2	0.28	–	0.9	–		100
90	0.86	33.1	–	66.9	0.64	–	1.3		traces	100
120	1.15	33.1	–	66.9	1.0	–	2.3	–	traces	100
150	1.93	33.7	–	66.3	1.3	–	2.6	–	0.96	99.1
180	2.23	34.8	–	65.2	1.5	–	2.8	–	1.04	99.0
210	2.63	38.9	–	61.1	2.0	–	3.2	–	2.5	97.5
240	3.0	40.8		59.2	2.3	–	3.4	–	3.0	97.0
270	3.34	42.8	–	57.2	2.9	–	3.8		3.9	96.1
B. $Ni/Ni_3C/NiO$										
30	8.5	48.8	8.3	42.9	8.1	1.7	7.1	16.0	0.98	82.9
60	9.7	44.2	5.4	50.3	8.1	5.9	9.3	15.5	2.6	81.9
90	10.9	44.8	4.5	50.6	10.1	5.0	11.5	12.9	3.8	83.2
105	13.3	44.8	4.6	50.6	12.0	6.2	13.5	11.6	6.2	82.2
Sample after SD + HP										
30	6.2	54.0	4.0	42.0	8.4	4.7	6.5	3.2	2.5	94.3
60	5.8	55.2	4.2	40.6	8.1	6.1	5.9	2.2	1.8	96.0
90	6.3	56.2	3.7	40.1	8.8	6.0	6.2	3.1	3.0	94.0
120	6.3	55.6	4.0	40.4	8.5	6.1	6.1	4.0	3.2	92.8
150	6.4	56.4	4.3	39.3	9.1	6.5	6.4	2.0	2.4	95.6
180	7.3	56.0	4.5	39.5	9.7	7.0	6.9	1.8	2.6	95.6
210	7.8	56.1	3.7	40.2	10.2	7.0	7.3	2.9	2.7	94.4
240	7.8	56.5	4.1	39.4	9.8	6.5	6.8	3.4	2.6	94.0

[a] A time count from the beginning of the run.
[b] Product distribution is based on the content of CH_4, C_2H_6, and CO_2 detected continuously at every run.

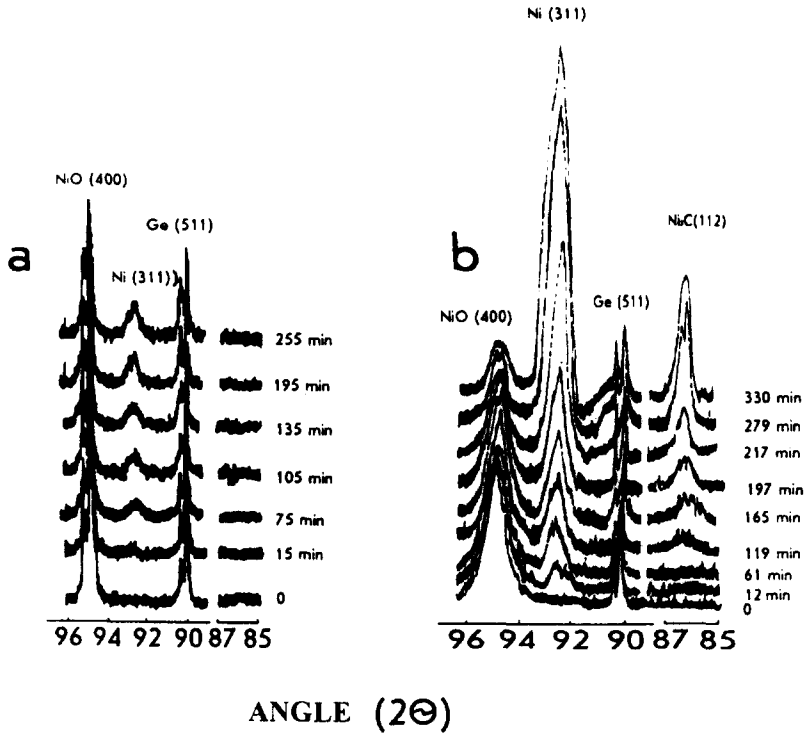

Fig. 3. In situ XRD spectra obtained during the reaction of a CO/H_2 mixture with (a) NiO(P-1) and (b) NiO(P-2) at 210°C.

observed this kind of clusters by TEM in a subsurface layer of a NiO particle. Reactions (2)–(4) were the contributors of $C_{intrinsic}$ being accumulated in the bulk of oxide. The reduction of the large microcrystals proceeded simultaneously with the changes in morphology. As a result, the Ni/NiO catalyst was formed.

At 255°C, the phase of Ni_3C was obtained in the Ni/NiO catalyst. The kinetic study of solid state reactions established that starting from this

Table 3
Dynamics of structural and catalytic properties of the initial 'plasmochemical' NiO sample and the sample subjected to shear deformation under high pressure, 255°C

t [a] (min)	Conversion CO (%)	Selectivity [b] (%)			Rate (mol s^{-1} m^{-2})			Phase composition (mol%)		
		CH_4	C_2H_6	CO_2	10^8 CH_4	10^{10} C_2H_6	10^9 CO_2	Ni	Ni_3C	NiO
Initial sample										
30	3.5	70.7	4.6	24.4	0.77	3.3	3.3	7.0		93.0
60	3.9	74.5	6.0	19.6	1.1	4.4	2.9	12.6	4.0	83.3
90	4.3	79.9	5.9	14.2	1.13	4.2	2.1	17.0	7.4	75.4
120	4.9	85.6	6.6	7.9	1.18	4.9	1.11	24.0	7.7	68.3
Sample after SD + HP										
30	4.0	44.5		55.5	0.84		10.7	8.6	8.8	82.6
60	3.7	45.7		54.3	0.82		9.4	6.5	7.3	86.2
90	3.9	48.0		52.0	0.84		9.0	5.8	6.2	88.2
120	3.8	51.2		48.8	0.89		8.6	5.6	5.7	88.7

[a] A time count from the beginning of the run.
[b] Product distribution is based on the content of CH_4, C_2H_6, and CO_2 detected continuously at every run.

temperature two pathways of NiO(P-1) transformation existed, as follows: the reduction into Ni(100) and the carbidization into polycrystalline Ni_3C [5]. The scheme for the formation of the Ni/Ni3C/NiO system was recently proposed in [5]. As we showed for the 'carbonate' samples, the orientation similarity between the structural elements of NiO and Ni_3C crystallographic units was extremely important for the formation of nickel carbide. Close inspection of the Ni/NiO system indicated that there were two places of Ni_3C formation. The first one was the interface between Ni and NiO, which was located lengthwise on the (111) plane of NiO and corresponded with the (111) plane of Ni. The second one was the stepped surface of the large NiO microcrystals, which was also located lengthwise on the (111) plane of NiO. The formation of Ni_3C required only the stoichiometric amount of carbon atoms accumulated on these surfaces through the diffusion of $C_{intrinsic}$ [11]

Thus, the sample consisting of the multigraded microcrystals of NiO covered by the epitaxial layers of Ni and polycrystalline Ni_3C was formed from the NiO(P-1) precursor.

The catalytic activity of the Ni/NiO catalyst in the CO hydrogenation was detected at 240°C. The dynamics of the structural and catalytic properties at 255°C is presented in Table 3. The changes in the phase composition result in an increase of the conversion of CO and of the rates of CH_4 and C_2H_6, formation. The rate of CO_2 formation decreases. The selectivity of CH_4 formation is found to be much higher than that for the catalyst being prepared from the NiO(C-1) precursor (Table 2). We propose that the (100) surface of Ni is specially suitable for the H_2 activation.

After the action of SD + HP, the reduction and carbidization of the NiO(P-2) sample begin at the same temperature, 210°C (Fig. 3b). We suggest that a rise in the temperature of reduction is associated with the effect of the dislocation network on the diffusion coefficients: magnetic measurements point to the presence of highly dispersed Ni clusters in the grain boundaries. According to TEM data, the bulk and surface distortions promote the formation of polycrystalline Ni instead of Ni(100) epitaxial layers being obtained on NiO(P-1). The reduction into Ni proceeds slowly during the first 120 min of the run. Then, the rate of the reaction rapidly increases. Simultaneously, the carbidization of both the NiO and polycrystalline Ni begins. The splits on the NiO microcrystals, which were located along the (111) plane, seem to be suitable for the Ni_3C formation because of the orientation similarity with the (0001) basal plane Ni_3C. The polycrystalline Ni is easily transformed into Ni_3C in a CO/H_2 mixture [6]. For these reasons, the carbidization of NiO(P-2) occurs at about 45°C lower than that of NiO(P-1).

Thus, the interaction of NiO(P-2) with a CO/H_2 mixture gives the $Ni/Ni_3C/NiO$ multicomponent sample containing the polycrystalline phases of Ni and Ni_3C. In response to the action of SD + HP, the regularity of the solid state reactions is changed.

Comparison of the data being obtained for the NiO(P-1) and NiO(P-2) samples demonstrates the dramatic changes in their catalytic properties (Table 3). In contrast to the 'carbonate' samples, the mechanically induced defects in the NiO(P-2) precursor lead to the degradation of the 'plasmochemical' catalyst in the CO hydrogenation. The rate of CO_2 formation increases sharply and becomes nearly equal to the rate of CH_4 formation. Therefore, the CH_4 selectivity reduces by $\sim 30\%$. No C_2H_6 is formed during the reaction. However, conversion of CO, as well as the rate of CH_4 formation, seem to be insensitive to system disturbances.

By TEM data, the $Ni/Ni_3C/NiO$ catalysts being prepared from NiO(P-1) and NiO(P-2) precursors vary in the morphology of the separate phases, as well as in the 'architecture' of the total samples. The surface of the $Ni/Ni_3C/NiO$(P-1) is found to be covered by the layers of Ni(100). Whereas, the polycrys-

talline metal does not form a continuous layer on the surface of the $Ni/Ni_3C/NiO$(P-2) due to the absence of the structural similarity with the (100) plane of NiO. Thus, the surface of the oxide and the Ni_3C/NiO interface are accessible for the reagents, as well as in the case of the $Ni/Ni_3C/NiO$ catalysts being prepared from NiO(C-1) and NiO(C-2) precursors. Of special interest is the correlation between catalytic properties of these samples indicating similar tendency: a high rate of CO_2 formation and, as a result, a low selectivity to hydrocarbons.

Thus, the change in the morphology of the Ni phase results in the drastic changes in the catalytic properties of the sample.

3.3. α-Fe_2O_3 sample

According to TEM data, the initial sample of α-Fe_2O_3 consists of sufficiently well packed 'monocrystalline' platelets with a layered structure. The (0001) basal plane is the best developed plane of the particles. Under the action of SD + HP, the number of defects in the crystallites increases considerably due to disturbances in the layer packing. Disordering of microblocks without crushing the particles as a whole is observed. Shearing and turning of the layers seem to occur in more than one direction [7].

The interaction of both samples with a CO/H_2 reaction mixture is found to be a two-stage process. On the first stage (270–285°C), hematite transforms into magnetite, Fe_3O_4. On the second stage (T > 300°C), the phase of χ-Fe_5C_3 is found to be formed. At 360°C, both samples include 50 mol% of Fe_3O_4 and 50 mol% of χ-Fe_5C_2. In spite of similar phase composition, the newly formed samples differ significantly in their 'architecture'.

According to the data of TEM and Moessbauer spectroscopy, the sample of nonstoichiometric magnetite (nonstoichiometric parameter $\delta = 0.02$) being prepared from the initial α-Fe_2O_3 consists of the polygonal platelets morphologically similar to those of the 'parent' oxide.

Reduction of the α-Fe_2O_3 sample subjected to SD + HP gives a nonstoichiometric magnetite whose oxidation state is high ($\delta = 0{,}09$). This sample contains disordered particles with a high cation vacancy concentration.

The extremely important is to visualize the 'architecture' of the χ-Fe_5C_2/Fe_3O_4 samples [7]. The χ-Fe_5C_2/Fe_3O_4 (I) consists of the well-crystallized particles of Fe_3O_4 with the (111) best developed plane. The inclusions of imperfect carbide are found to penetrate the bulk of the magnetite particle. Each particle of the intercalated oxide/carbide system is surrounded by a thin layer (up to 100 Å) of amorphous carbon. The χ-Fe_5C_2/Fe_3O_4 (II) consists mainly of the imperfect Fe_3O_4 particles covered with carbon precipitates. The loose aggregates of χ-Fe_5C_2 and some amount of coke are also occur.

Fig. 4 demonstrates the integral kinetic curves describing the changes in the phase composition of the samples and in the conversion of CO to the C_1–C_4 hydrocarbons at non-steady-state conditions. Initial catalytic activity in the CO hydrogenation was detected for the magnetite samples. On this stage, the Fe_3O_4(II) sample with the disordered particles and high vacancy concentration demonstrates the catalytic activity nearly twice higher than that of the Fe_3O_4(I). Thus, the mechanically induced defects in the precursor improve the catalytic properties of the Fe_3O_4 samples. The further solid-phase transformation results in degradation of the 'active' catalyst and in improvement of the 'low-active' one.

The role of 'architecture' of the catalyst is most conspicuous on this stage. For the formation of hydrocarbons from CO and H_2, the sample with the well-crystallized Fe_3O_4 particles penetrated by the carbide inclusions is found to be favored over the sample consisting of the Fe_3O_4 particles surrounded with the carbon precipitates and loose aggregates of χ-Fe_5C_2, in spite of similar phase composition of both cata-

lysts. The disruption of spinel lattice hesitates development of the well-oriented carbide layers. We assume that the loose aggregates of carbide and lamella of carbon reduce the catalytic activity preventing the access of reactants to the active surface.

Although our experimental data do not allow the derivation of any kind of relationships between the catalytic properties and surface structure of the samples, it is interesting to compare briefly the results obtained with the recently published studies performed on similar systems.

The catalytic features observed for $Ni/Ni_3C/NiO$(P-1) sample are in a good agreement with those observed for supported and polycrystalline metal catalysts, as well as for the single crystal metal planes [14–20]. This is not surprising since the duality is an inherent property of the system: from the one side, it is a supported catalyst consisting of metal Ni (up to 24 mol%) supported on NiO; from the other side, it is a model of the Ni(100) single crystal surface [6]. However, we found no evidence that the N_3C phase is an intermediate in the CO hydrogenation.

Contrary to $Ni/Ni_3C/NiO$(P-1), the Ni_3C/NiO(C-1), $Ni/Ni_3C/NiO$(C-2), and $Ni/Ni_3C/NiO$(P-2) samples exhibit completely different properties (Tables 2 and 3). The rate of CO_2 formation is found to be nearly the same, as the rate of CH_4 formation, that is unusual for the Ni-containing catalysts. Similar results are

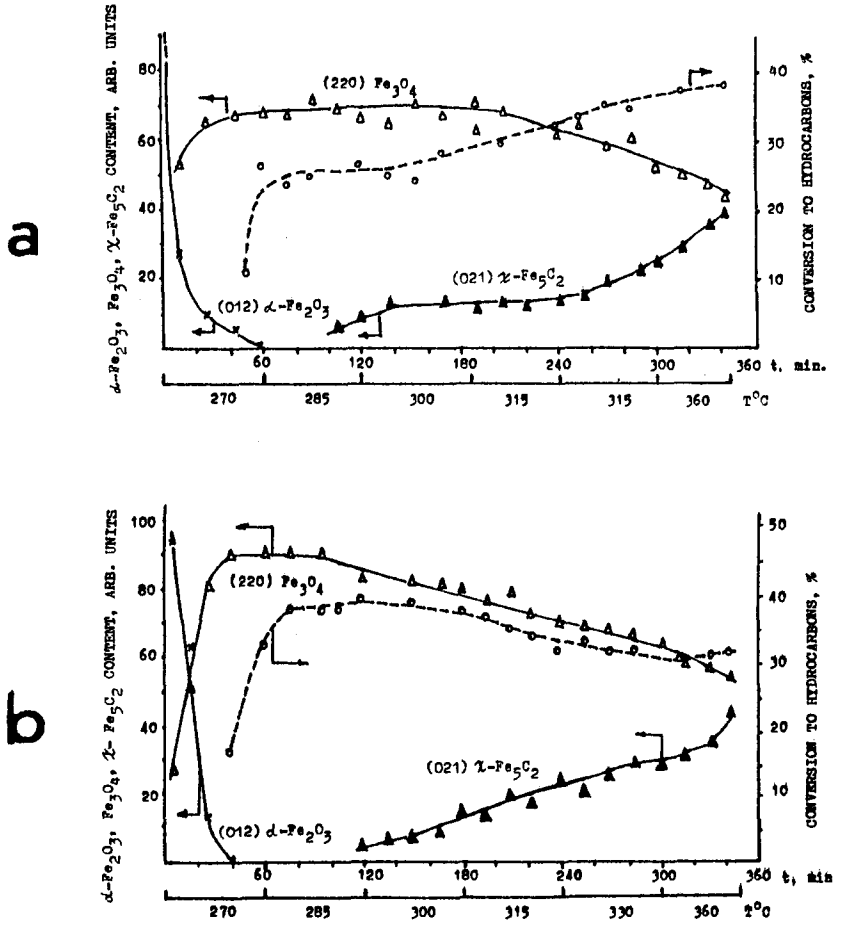

Fig. 4. Change in the integral intensities of α-Fe_2O_3(012), Fe_3O_4(220), and χ-Fe_5C_2(021) and variation in the conversion of CO to hydrocarbons obtained for the α-Fe_2O_3(I) (a) and α-Fe_2O_3(II) (b).

obtained for χ-Fe_5C_2/Fe_3O_4: the rate of CO_2 formation is equal to or higher than the total rate of C_1–C_4 hydrocarbons formation. Thus, the χ-Fe_5C_2/Fe_3O_4 and Ni_3C/NiO(C-1) samples containing only carbide and oxide phases of special morphology and carbon inclusions are very similar in their catalytic behavior. Through this phenomenon of particular interest, we demonstrate that the catalytic properties strongly depend on the phase composition of the catalyst. As for the Fe-containing catalyst, these data satisfactorily correlate with the stoichiometry commonly observed: $2CO + 2H_2 \rightarrow CH_4 + CO_2$ [21,22]. A major portion of CO_2 can be produced by the Bell–Boudouard reaction, as well as by the water–gas shift reaction and partial reduction of iron oxide giving new adsorption centers, e.g. anion vacancies [14,21,7]. The low hydrogenation activity due to deficiency of the centers for H_2 activation leads to the deposition of carbide carbon or surface carbide overlayers [6,7,19,23]. The Ni-containing catalysts seem to be unsuitable for the water–gas shift reaction; instead, carbide carbon reacts with H_2O giving CO_2 [14,24]. We suppose that the hydroxyl groups covering the oxide surfaces [25–28] also take part in the CO_2 formation. These groups are found to be particularly stable on NiO(111). The OH coverage is by a factor of 3 larger on NiO(111), as compared to NiO(100) [25,26]. The OH groups may participate in the formation of formates on the NiO surface during the treatment in a CO/H_2 mixture [4,14,27,29,30]. At the low hydrogenation activity, decomposition of formates, as well as carbonates, leads to CO_2 formation. Also, CO_2 is produced by the reaction of hydroxyl groups with carbonyl species, [31].

The above-mentioned explanation for the unusual behavior of Ni_3C/NiO(C-1) catalyst in the CO hydrogenation is not faultless for the Ni/Ni_3C/NiO(C-2) and Ni/Ni_3C/NiO(P-2) samples because the Ni present in the catalyst facilitates H_2 activation. Consequently, it is our goal to study the reactivity of surface species on all of these samples in the near future.

4. Conclusion

The initial microstructure and morphology of the polycrystalline iron and nickel oxide precursors are of fundamental importance in the processes of the catalyst preparation. The structural peculiarities of original oxides have a pronounced effect on the phase composition, 'architecture', and the catalytic properties of the newly formed multicomponent samples. Disrupting the oxide microstructure, we violate the direction and regularity of the solid state reactions. As a result, the structural and catalytic properties of the multiphase catalysts vary. The role of mechanically induced structural defects in improving the catalytic properties of the samples being formed is open to speculation.

References

[1] H.R. Oswald and J.R. Gunter, in P. Barret and L.C. Dufour, Editors, Reactivity of Solids, Materials Science Monographs, Vol. 28A, Elsevier, Amsterdam, 1985, pp. 101–108.
[2] B. Lamine, M Leseur and B. Pieraggi, in P. Barret and L.C. Dufour, Editors, Reactivity of Solids, Materials Science Monographs, Vol. 28A, Elsevier, Amsterdam, 1985, pp. 899–903.
[3] J.B. Benziger, V.V. Guliants and S. Sundaresan, Proc. 210th ACS Symp. Catal. Photocatal. Metal Oxides, Chicago, 1995, Abstr., 0.38.
[4] A. Boudriss and L.C. Dufour, in J. Nowotny and W. Weppner, Editors, Nonstoichiometric Compounds, Surfaces, Grain Boundaries and Structural Defects, Kluwer Academic, London, 1989, p. 311.
[5] O.S. Morozova, G.N. Kryukova, D.P. Shashkin, L.M. Plyasova and O.V. Krylov, J. Catal., 158 (1996) 13.
[6] O.S. Morozova, A.V. Ziborov, G.N. Kryukova and L.M Plyasova, J. Catal., 144 (1993) 50.
[7] O.S. Morozova, Y.V. Maksimov, D.P. Shashkin, P.A. Shiryaev, V.V. Matveev, V.A.Zhorin, O.V. Krylov and G.N. Kryukova, Appl. Catal., 78 (1991) 227.
[8] V. Parkhomenko and P.N. Tsybulev, Proc. 8th Int. Symp. Plasmochem., Tokyo, Vol. 4, 1987, p. 2105.
[9] D.P. Shashkin, M.Ya. Kushnerev, P.A. Shiryaev and O.V. Krylov, Kinet. Katal., 23 (1982) 1280.
[10] R.P. Adler, H.M. Otte and G.N. Wagner, J. Met. Trans.,1 (1970) 2375.
[11] G.R. Darling, J.B. Pendry and R.W. Joyner, Surf. Sci., 221 (1989) 69.
[12] G.N. Kryukova, Ph.D. Thesis, Moscow, 1989.
[13] M.I. Buckett and L.D. Marks, Surf. Sci., 323 (1990) 353.
[14] R.D. Srivastava, Heterogeneous Catalytic Science, CRC Press, Boca Raton, FL, 1988, pp. 93–120.

[15] S.Z. Ozdogan, P.D. Gohis and J.L. Lanconer, J. Catal. 83 (1983) 257.
[16] C.H. Bartholomew and C.K. Vance, J. Catal., 91 (1985) 78.
[17] M. Araki and V. Ponec, J. Catal., 44 (1976) 439.
[18] D.W. Goodman, R.D. Kelley, T.E. Madey and J.T. Yates, Jr., J. Catal., 63 (1980) 226.
[19] J. Nakamura, H.Hirano, M. Xie, I. Matsuo, T. Yamada and K.-i. Tanaka, Surf. Sci., 222 (1989) L809.
[20] H. He, J. Nakamura and K.-i. Tanaka, Surf. Sci., 283 (1992) 117.
[21] J.P. Reymond, P. Meriandeau and S.J. Teichner, J. Catal., 75 (1982) 39.
[22] H.J. Krebs and H.P. Bonzel, Surf. Sci., 88 (1979) 269.
[23] T. Aizawa, R. Sonda, S. Otany, Y. Ishizawa and C. Oshima, Phys. Rev., B42 (1990) 11469.
[24] J.A. Rabo, L.F. Elek and J.N. Francis, Stud. Surf. Sci. Catal., 7 (1981) 490.
[25] F. Winkelman, S. Wohlrab, J. Libuda, M. Baumer, D. Cappus, M. Mendes, K. Al-Shamery, H. Kuhlenbeck and H.-J. Freund, Surf. Sci., 307/309 (1994) 1148.
[26] D. Cappus, M. Haβel, E.Neuhaus, M. Heber, F. Rohr and H.-J. Freund, Surf. Sci., 337 (1995) 268.
[27] J. Wanmbach, G. Illing and H.-J. Freund, Chem. Phys. Lett., 184 (1991) 239.
[28] S. Bourgeois and M. Perdereau, Surf. Sci., 117 (1982) 165.
[29] M.-Y. He and J.G. Ekerdt, J. Catal., 87 (1984) 381.
[30] F. Solymosi, T. Bansagi and A. Erdoehelyi, J. Catal., 72 (1981) 166.
[31] Y. Iwasawa, Adv. Catal., 35 (1987) 181.